Med Biol Eng Comput
DOI 10.1007/s11517-008-0347-6

ORIGINAL ARTICLE

Constraining the general linear model for sensible hemodynamic response function waveforms

Koray Çiftçi · Bülent Sankur · Yasemin P. Kahya · Ata Akın

Received: 6 December 2007 / Accepted: 2 April 2008

Abstract We propose a method to do constrained parameter estimation and inference from neuroimaging data using general linear model (GLM). Constrained approach precludes unrealistic hemodynamic response function (HRF) estimates to appear at the outcome of the GLM analysis. The permissible ranges of waveform parameters were determined from the study of a repertoire of plausible waveforms. These parameter intervals played the role of prior distributions in the subsequent Bayesian analysis of the GLM, and Gibbs sampling was used to derive posterior distributions. The method was applied to artificial null data and near infrared spectroscopy (NIRS) data. The results show that constraining the GLM eliminates unrealistic HRF waveforms and decreases false activations, without affecting the inference for "realistic" activations, which satisfy the constraints.

Keywords Near infrared spectroscopy · General linear model · Gibbs sampling · Hemodynamic response function · Stroop test

1 Introduction

Detection of activation from neuroimaging data comprises the search for consistent and plausible waveforms from the recorded time series. This is typically accomplished by assuming a hypothetical waveform for the HRF and checking the degree to which this waveform manifests itself in the measurements. Canonical HRF (cHRF), which is composed of the difference of two gamma functions, is commonly used for this purpose [13]. Since mismatches between the hypothetical and actual waveforms can substantially decrease the detection performance, some flexibility is allowed in the basic model in order to better capture the variations in the hemodynamic response. Employing temporal and dispersion derivatives (TD and DD) along with the cHRF is one of the most common ways to attain a more robust analysis [13]. Accordingly, the HRF is modeled as a linear combination of three waveforms. However, even if a successful waveform modeling is apparently obtained, there is still a concern about the reliability of the analysis and it should be checked whether it represents a plausible HRF or not. Obviously if there are no restrictions on the linear combination weights, then unrealistic HRFs may be obtained, and consequently activations may be detected when there are none.

Constraining the basis set for modeling the HRF has been studied using variational Bayes [27], where basis waveforms were formed via singular value decomposition of a set of plausible HRF sample waveforms. Then using regression analysis, a multivariate normal distribution was fitted for the basis weights and this information was used as prior distribution in the Bayesian analysis. This was a "soft-constraint" approach in the sense that multivariate normal could not capture all details of the true distribution. Despite this limitation, this work has shown that constraining the basis set allowed for superior separation of active voxels from non-active voxels in fMRI data. The method of constraining the linear combinations of the basis set has also been taken up in the canonical correlation analysis framework [12]. The limitation of this work,

K. Çiftçi (✉) · A. Akın
Institute of Biomedical Engineering, Boğaziçi University, Istanbul, Turkey
e-mail: rciftci@boun.edu.tr

B. Sankur · Y. P. Kahya
Department of Electrical and Electronics Engineering, Boğaziçi University, Istanbul, Turkey

however, is that only positivity of the linear combination coefficients is required.

In this work, we propose a method for doing constrained parameter estimation and inference using the GLM in a Bayesian framework. Using the canonical basis set, (cHRF, TD, DD), an admissible region is defined in the three-dimensional weight space, and Gibbs sampling is used to arrive to posterior distributions. More explicitly, in our approach we specify uniform prior distributions for the parameters. The support of those uniform distributions represents our a priori knowledge, and thus we are sure that the parameter estimates belong to the feasible set. Since, we do not introduce a new basis set, but rather use the canonical basis set, it is a direct extension of the commonly used GLM for neuroimaging.

The feasibility of the proposed method is tested in the context of NIRS, which is an emerging neuroimaging tool. NIRS measures the relative concentration changes of oxygenated and deoxygenated hemoglobin using light within the near-infrared wavelengths [26]. There are numerous studies where functional magnetic resonance imaging and near infrared spectroscopy data are simultaneously acquired and the estimated hemodynamic responses are compared [18, 24]. Although there is a commonly accepted canonical HRF waveform, the instantiations of observed effects can differ in terms of rise time, undershoot, delay, duration etc. We expect that the constrained HRF estimation will be more effective for NIRS analysis, on one hand, by allowing controlled variations around a canonical HRF that was tailored for fMRI, and on the other hand by leading to a better assessment of the cognitive activity via fNIRS. In summary, constraining the GLM may enable us to be flexible enough to cope with variations in the HRF waveform, but also stringent enough not to allow unrealistic HRF shapes.

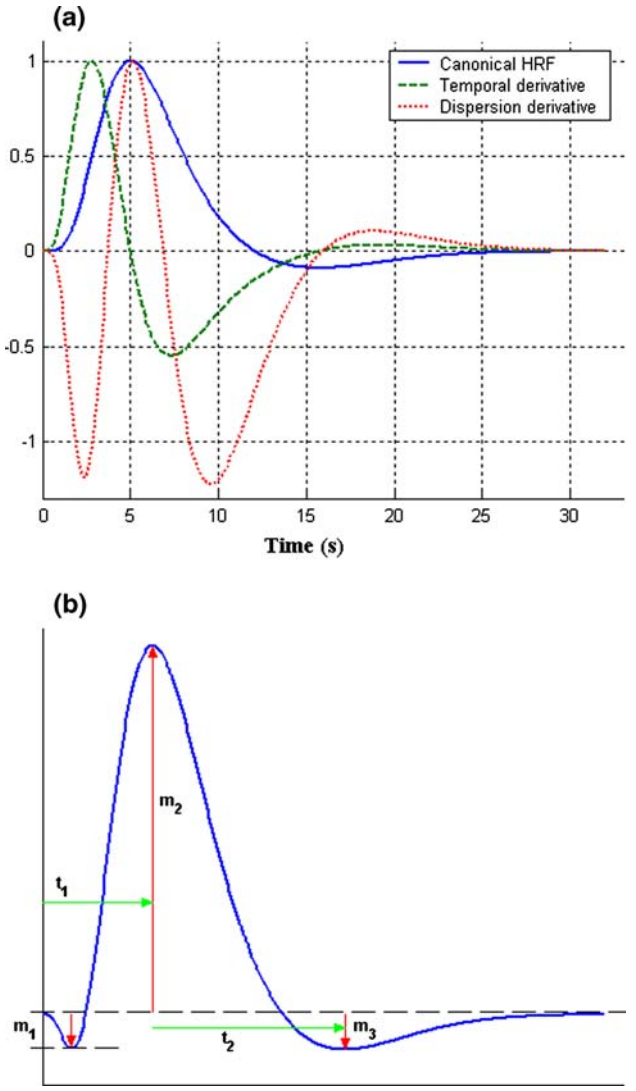

Fig. 1 **a** Canonical HRF with its temporal and dispersion derivatives (maximum value scaled to unity). **b** Parameters that characterize the HRF: t_1 time to peak, t_2 time to undershoot from peak instant, m_1 magnitude of initial dip, m_2 magnitude of main response, m_3 magnitude of undershoot

2 Materials and methods

2.1 Constraining the basis set

The canonical basis set is reproduced in Fig. 1a, where the peak values of the waveforms are scaled to unity. Sample HRF waveforms were generated by varying the coefficients of the two derivative terms in linear combinations. The resulting waveforms were tested for their plausibility and a tally of the coefficients that satisfied these criteria was kept. An HRF is shown in Fig. 1b with the parameters that characterize its main features. The setting of parameter ranges was based on information gleaned from the literature on temporal dynamics of the HRF [4, 7, 17] and the work on constrained basis sets [27]. An alternative might be using a physiological model, like the balloon model [3], and obtain sample HRFs from this model. The criteria used in determining the plausible HRF waveforms can be listed as:

- A main response with a peri-stimulus time of 3–8 s: $3 < t_1 < 8$;
- Not more than one positive peak;
- Not more than two negative dips;
- An initial dip with magnitude not greater than quarter of the magnitude of the onset: $0 < m_1 < m_2/4$;
- An undershoot after 2–8 s after the main peak: $2 < t_2 < 8$;
- Magnitude of the undershoot not greater than half of the magnitude of the onset: $0 < m_3 < m_2/2$.

Figure 2a shows the feasible region of TD and DD coefficients. The nonrectangular shape of the feasible region indicates that TD and DD coefficients are statistically dependent. Figure 2b shows the plausible HRF waveforms obtained by sampling the permissible TD–DD region.

Since the activation is defined as an increase of oxy-Hb and a decrease of deoxy-Hb, the coefficient of the cHRF is expected to be positive. The NIRS device measures the concentration value in molar units, and the coefficient of the cHRF is constrained to be between 0 and 5 μM. This range is broader than typical cognitive activation magnitudes in the prefrontal cortex found in several NIRS studies [21, 25]. For deoxy-Hb, the time series can be inverted in sign and the same constraints can be applied. The constraints on these three parameters then define a volume in 3-D space.

2.2 Bayesian analysis of the constrained GLM

The basic GLM is formulated as, $Y = X\beta + Zh + e$, where Y is the N-sample vector of NIRS data (oxy-Hb or deoxy-Hb), X is the $N \times p$ design matrix, β is the p vector of parameters for effects of interest, Z is the $N \times q$ design matrix, h is the q vector of parameters for nuisance effects, and e is the N-long noise vector. Y, X and Z are known and β, h and e are unknown. In the Bayesian analysis of the GLM, priors are specified for the unknown variables and posterior distributions are derived. The constraints for β, effectively the priors of β, have already been defined in the previous section. To complete the Bayesian analysis, we have to specify priors for h and e. Since we have no prior information about nuisance effects, we will set their prior to uniform distribution: $p(h) \propto uniform$. The noise is assumed to be uncorrelated, zero-mean, Gaussian distributed with variance σ^2, for which the Jeffreys (non-informative) prior is used: $p(\sigma^2) \propto \sigma^{-2}$. Using Bayes rule, full conditional posterior distributions for the variables are found so that Gibbs sampling can be used to generate sample values from the posterior. At each sampling instance, the feasible intervals for the elements of the β vector are imposed. Note that the posterior of the β vector is just the truncated version of the likelihood, since $p(\beta/Y) = p(Y/\beta)p(\beta)$, and $p(\beta)$ acts like a range delimiter. We can use the technique introduced in [6] to draw samples from this truncated distribution: If F_i is the likelihood function for β_i, and U is a uniform (0,1) variate, then $\theta_i = F_i^{-1}[F_i(a) + U(F_i(b) - F_i(a))]$ is a random variate from the truncated likelihood (posterior), where the feasible interval for β_i is [a b]. The execution of the Gibbs sampling can be summarized as below:

1. From $i = 1{:}p$, sample β_i from $p(\beta_i \mid \beta_{-i}, h, \sigma^2)$, where by convention β_{-i} denotes all the β parameters except the ith one,
2. Sample h from $p(h \mid \beta, \sigma^2)$,
3. Sample σ^2, from $p(\sigma^2 \mid \beta, h)$.

Since we are assuming additive Gaussian noise, the likelihood function also has a Gaussian form. Hence, the distribution in the first step is a truncated univariate Gaussian; the distribution in the second step is a multivariate Gaussian and in the last step it is inverse Gamma distributed. After obtaining the posterior distribution of the parameters given the observations, we can use these posteriors to make inferences about the parameters and the related events. In the execution of Gibbs sampling, the chain was run for 10,000 iterations and the first 2,000 iterations were discarded as burn-in. Then, the marginal posterior distribution can be obtained by smoothing the sample-based histogram with a Gaussian kernel.

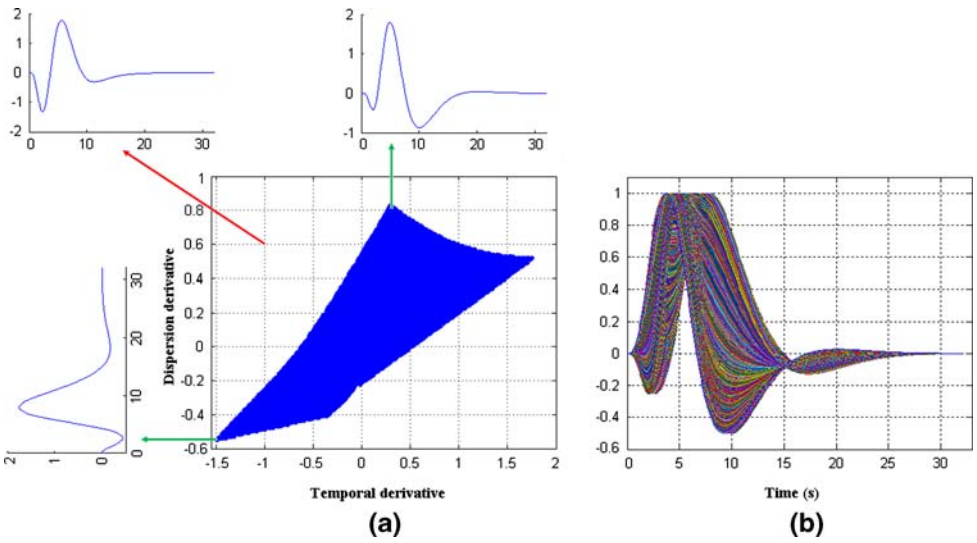

Fig. 2 **a** Feasible values for the coefficients of the derivative terms with two instances of admissible waveforms and one non-admissible waveform. **b** The set of plausible HRF waveforms (maximum values scaled to unity)

The analyses were conducted using MATLAB® v6.5 and run time for one subject was approximately 3 min on a PC equipped with Pentium® 4 (2.40 GHz) CPU and 512 MB of RAM.

2.3 NIRS data acquisition and experimental setup

NIRS data were recorded from 15 volunteers (8 male, age 26.5 ± 4.7 years) recruited from the university community. Subjects had no reported neurological, medical and psychiatric disorders. None were taking medications at the time of measurement. Written informed consent was obtained from all subjects before the measurement.

Experiments were performed using a continuous-wave near-infrared spectroscopy device NIROXCOPE 301, (Hemosoft Inc., Ankara Turkey) [1, 2]. The device is capable of transmitting near-infrared light at two wavelengths (730 and 850 nm), which are known to be capable of penetrating through the scalp and probe the cerebral cortex. Calculation of concentration changes of oxy-Hb and deoxy-Hb in blood is based on modified Beer-Lambert law [5]. Employing 4 light-emitting diodes (LEDs) and 10 detectors, the device can sample 16 different volumes (channels) in the brain simultaneously. The distance between each source and detector is 2.5 cm, which guarantees a probing depth of approximately 2.0 cm from the scalp. This amount of separation has been shown to reliably probe the cortical activity [10, 11]. LEDs and detectors were placed in a flexible printed circuit board that was specially designed to fit the curvature of the forehead. Sampling frequency of the device was 1.4 Hz.

NIRS data were obtained from the prefrontal cortex of the subjects during color-word matching Stroop task [30]. Subjects were presented with two words, one above the other. The top one was written in ink-color whereas the bottom one was white presented over a black background. Subjects were asked to decide whether or not the word written below correctly denoted the color of the upper word. If color and word matched, then subjects were asked to press the left mouse button with their forefinger; if not, the right mouse button with their middle finger. Subjects were informed to perform the task as quickly and correctly as possible. The words stayed on the screen until the response was given within a maximum duration of 3 s. The screen was blank between the trials.

The experiment consisted of neutral, congruent and incongruent trials. In the neutral condition the upper word consisted of four X's (XXXX) in ink-color. In the congruent condition ink-color of the upper word and the word itself were the same, whereas in the incongruent condition they were different. The trials were presented in a semi-blocked manner. Each block consisted of six trials. Inter-stimulus interval within the block was 4.5 s and the blocks were placed 20 s apart in time. The trial type within a block was homogeneous (but the arrangements of false and correct trials were alternating) There were ten blocks of each type. Experiments were performed in a silent, lightly dimmed room. Words were presented via an LCD screen that was 0.5 m away from the subjects. The task protocol has been approved by the Ethics Review Board of Boğaziçi University.

3 Results

To put into evidence the role of constrained GLM vis-a-vis unconstrained GLM, we ran two sets of experiments. We denote these two approaches, respectively, in a more suggestive way, as the Bayesian approach and the non-Bayesian or frequentiest approach. In the first experiment, we applied the algorithm on null hypothesis data, where we expect the Bayesian approach to yield low significance values while the frequentiest approach strives to model events even where there are none. Conversely, the Bayesian approach is expected to yield higher reliability scores on the alternative hypothesis data, that is, when there is an event. In classical analysis, the effect sizes for different contrasts are tested against zero. Since in the constrained analysis the coefficient of the cHRF has already been restricted to be positive, a "difference contrast" should be used. On the other hand, since Bayesian analysis gives us posterior distributions, it is possible to define a threshold other than zero, and make inference even in one stimulus case. In our experiments with artificial and real data, we used experimental paradigms with more than one stimulus.

Inference for activation was based on the main component (cHRF) while the two derivative terms (TD and DD) modeled the variations in the basic HRF, that is, we produced the associated T statistic for cHRF to test the activation. An alternative might be to investigate the total power explained by the linear combination of the basis functions with an F statistic. However it is known that F statistic is always less sensitive and T statistic based on the cHRF is recommended, especially when the shift in the HRF is known to be less than 1 s [29].

3.1 Artificial null data

Ten thousand artificial null data were generated using Gaussian noise and a number of trend terms simulating the background activity. We designed a thought-experiment with two stimuli in an event related setting with inter stimulus interval of 20 s. Forming a design matrix using cHRF, its derivatives and discrete cosine transform

functions for modeling the linear trends (nuisance part), the parameters were estimated using both unconstrained ordinary least squares (OLS) and constrained Bayesian analysis. Finally, the z-statistics of the contrast between the cHRF parameter values of the two stimuli were calculated. The z-statistics (or pseudo-z-statistics [27]) were obtained from the marginal posterior for the constrained case. Figure 3a shows the histogram of z-statistics obtained for the artificial null data for the two analysis cases. It can be observed that the z-histogram is more concentrated around 0 for the constrained case. The reason is that constraining the basis set penalizes the unlikely parameter values and lowers their significance. The log–log probability plot in Fig. 3b shows the probabilities under the tail for a given z-statistic for both frequentiest (unconstrained) and Bayesian (constrained) analysis. It may be observed that the empirical frequentiest probabilities are in conformance with the theoretical probability values, that is, the z-scores one would obtain in pure noise, whereas the Bayesian analysis produces much smaller probabilities. This means that constraining the basis set reduces false activations.

3.2 NIRS data

Reaction times for the neutral, congruent and incongruent trials were $1{,}028.9 \pm 193.2$, $1{,}160.6 \pm 265.6$ and $1{,}260.9 \pm 242.1$ ms, while the error rates were 0.22 ± 0.86, 1.33 ± 2.11 and 4.00 ± 4.58, respectively. Since error rates were small, we calculated the interference effect (incongruent $-$ neutral) only in terms of reaction times. There was a clear interference effect with $P < 0.0001$. The difference between the reaction times of incongruent and congruent trials and congruent and neutral trials were also significant ($P < 0.01$).

Since interference effect is known to be well pronounced in Stroop task [19], which has also manifested itself in our behavioral analysis, we decided to concentrate on this contrast for hemodynamic response results. Although NIRS can measure both oxygenated and deoxygenated hemoglobin, we used only oxygenated hemoglobin, since our previous studies in agreement with the literature, showed that oxygenated hemoglobin was a more sensitive indicator of cognitive activity in the prefrontal cortex during Stroop task [9].

In the GLM to analyze NIRS data, the design matrix (X) consisted of the cHRF and its derivatives convolved with the stimulus onset vectors for each type of trial. The design matrix modeling the nuisance effects (Z) consisted of discrete cosine transform functions to cope with various low-frequency trends [14]. Incorrect and omitted trials were modeled separately and included in the design matrix as nuisance effects. In other words, inference was based on only correct trials. Each channel of each subject was analyzed individually.

Figure 4 shows the histogram of z-statistics for the unconstrained and constrained cases for the overall data, 15(subjects) $\times$ 16(channels), for the interference effect. It may be observed that, as it was the case with the artificial null data, histogram is denser for low z values (-2 to 2) under constrained estimation. The reason is that constrained linear combinations preclude unlikely parameter occurrences. At the same time, the constrained histogram has higher absolute z-values at both ends, since in the case of strong activations and deactivations that satisfy the constraints, our method yields lower variance estimates, which in turn causes the significance scores to increase. Figure 5 shows the activation matrix (subject $\times$ detector) for OLS and Bayesian analysis. It may be seen that the activation maps, consisting of the 16 measurements of the 15 subjects are similar to each other. One can observe that the constrained analysis results in some deleted activation cells while new activations are added. For instance, while frequentiest inference does not result in any activation for the 11th subject, constrained analysis identifies three active channels at the left lateral cortex. Figure 6 explains the reason for this phenomenon. The recording shown is from the fourth channel of the 11th subject. In Fig. 6a, the fitted waveforms with the unconstrained and constrained

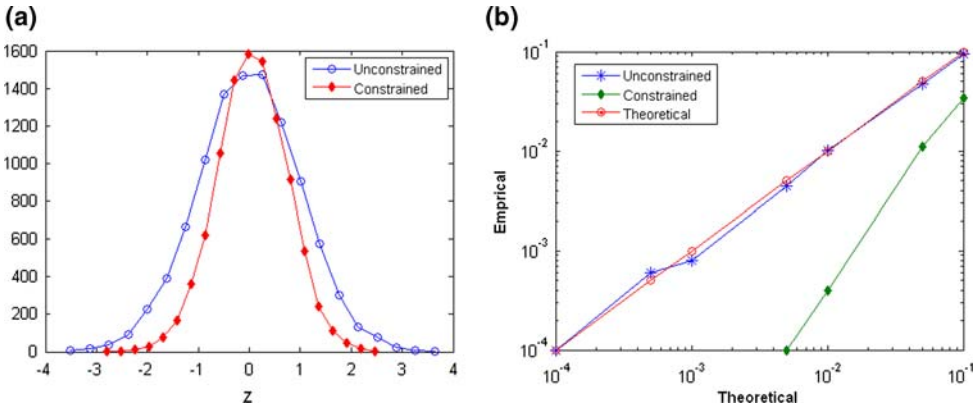

Fig. 3 **a** Histograms of the z-statistics for the unconstrained and constrained analysis from artificial null data. **b** Log probability–log probability plots for the tail masses of theoretical and empirical (constrained and unconstrained) cases

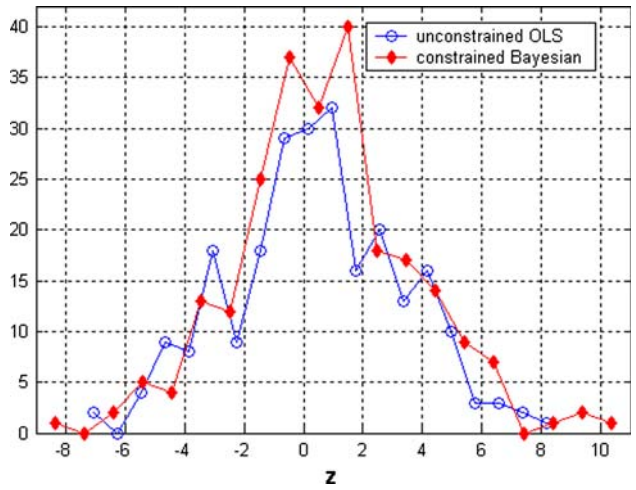

Fig. 4 Histograms of the z-statistics for the unconstrained and constrained analysis of NIRS data

approaches are superimposed. The actual NIRS recording is very noisy and there is a continuous oscillation that hides the activation. In the unconstrained case, the OLS estimate tries to fit the model to these oscillations by increasing the derivative terms and suppressing the canonical HRF. On the other hand, constrained estimate is not allowed to increase the derivative terms without limit and finds the best fit that satisfies the constraints. The result is that, it models the variations in the basic HRF shape, but does not model the spurious oscillations and reveals the activation that OLS was not able to identify. Note that we are testing for the contrast "incongruent–neutral". Although the difference between unconstrained and constrained cases seems to be more evident for congruent blocks, there is a subtle difference for incongruent blocks. The coefficients estimated for the cHRF, TD and DD by unconstrained analysis for incongruent trials are 0.079, 0.436 and 0.163, respectively. The same coefficients are estimated as 0.228, 0.294 and 0.085 by the constrained analysis. Figure 6b shows the HRF waveforms generated by these coefficients. Note that the main response is similar and hence there seems to be only a minor difference between the two cases in Fig. 6a. However, the unconstrained analysis produces an implausible HRF with the coefficient of the cHRF being very small, whereas constrained analysis captures the same main response with cHRF and cannot increase derivative terms to make the waveform implausible. Consequently, the tested contrast becomes significant for constrained analysis. Hence, constraining the GLM improves the estimates in two opposite directions: It eliminates the activations due to nonsensible HRF waveforms and it brings forth activations that would otherwise remain hidden.

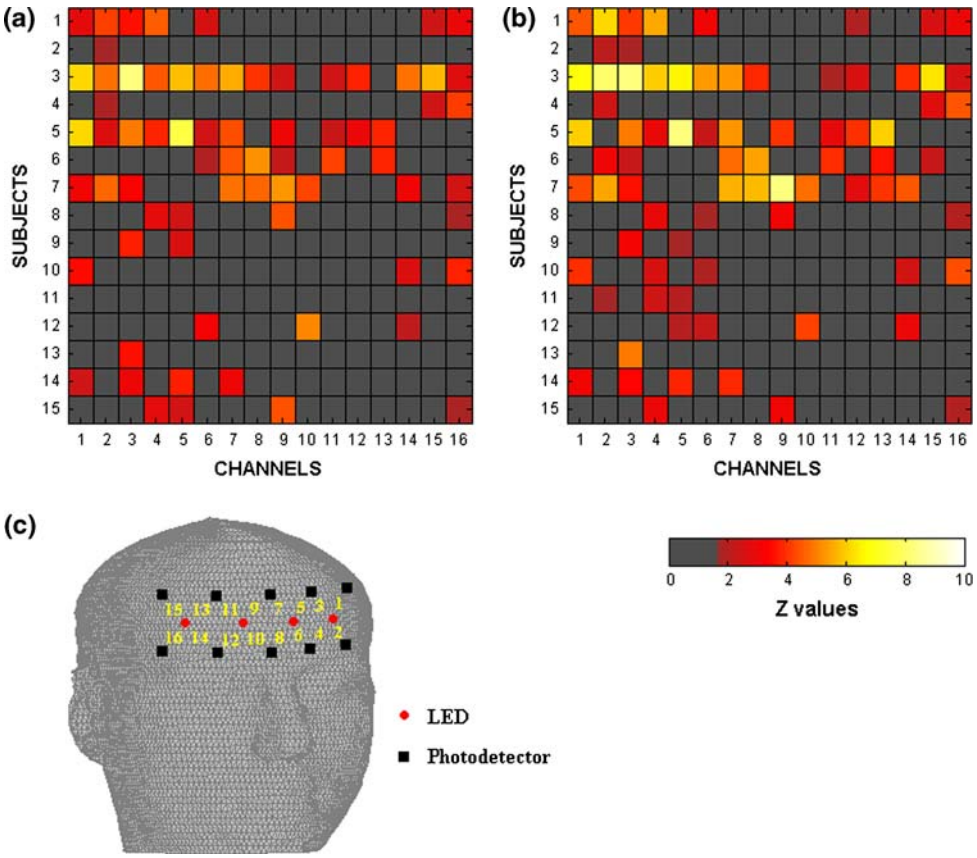

Fig. 5 Activation matrix (subjects × channels) thresholded at $P = 0.05$ ($z = 1.65$), for **a** unconstrained, **b** constrained analysis. **c** Placement of the LEDs and photodetectors; channel locations are depicted with numbers

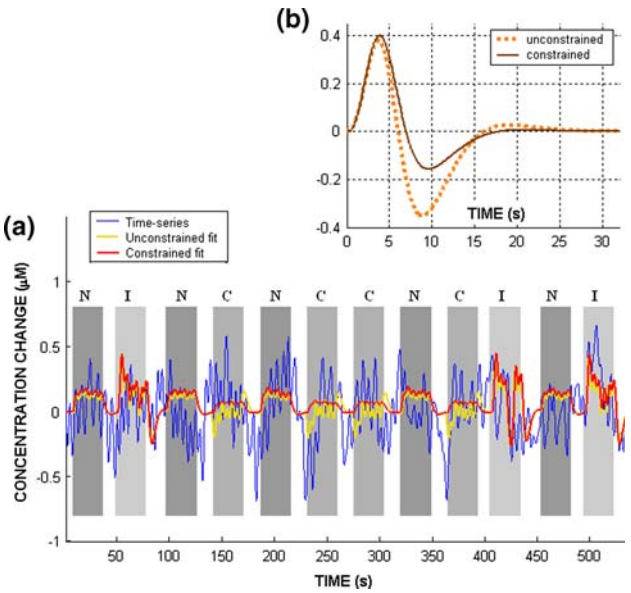

Fig. 6 **a** Fitted waveforms to a noisy NIRS signal under constrained and unconstrained analyses (*N* neutral, *C* congruent, *I* incongruent trial blocks). **b** Estimated HRF waveforms for incongruent stimulus

Figure 7 shows the HRF waveforms of incongruent trials obtained from the activated channels by constrained and unconstrained analysis. It may be seen that most of the waveforms remain unchanged but the unrealistic HRF shapes are eliminated.

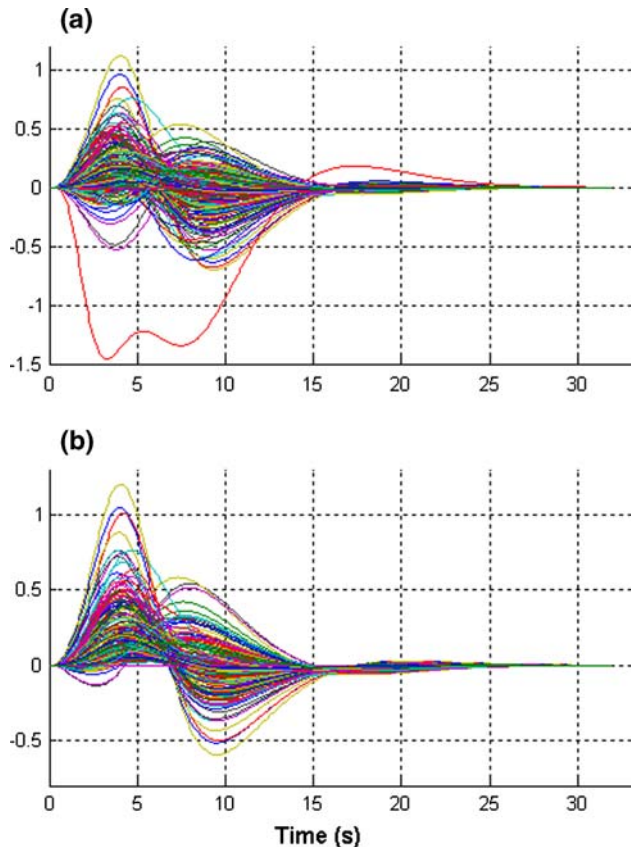

Fig. 7 HRF waveforms of the incongruent trial for the activated channels obtained by (**a**) unconstrained and (**b**) constrained analysis

4 Discussion

The method presented in this study is a direct extension of the classical GLM analysis with the main difference being the constraints put on the solution space to ensure that the resulting HRF is physiologically plausible. The Bayesian methodology enters into the play to constrain the estimation of the parameter vector. We want to emphasize here that our study does not overlook the importance of the exploratory methods. Nevertheless, as the name implies, GLM is a model-based approach and constraining the solution space is a way to ensure that this model really holds.

In another seminal work [27], a method for constraining the linear combination of basis sets using variational Bayes was introduced. In that work, a set of plausible HRF waveforms were generated and the basis set that best spanned these waveforms was found. In contrast, rather than developing a new model, we simply propose an "option" for classical GLM analysis. In other words, we consider the basis set as given and then find all the plausible HRF waveforms that might be generated with it. Consequently, we adopt a "hard-constraint" approach in the sense that the prior for the parameter vector is specified as a range-limiting uniform distribution. In the Bayesian analysis, uniform prior distributions or indicator functions give rise to truncated posterior distributions, and the latter can be easily inferred upon by Gibbs sampling [8, 15, 22]. In this study, we use a simple method to generate samples from a truncated distribution in univariate cross sections [6]. This allowed us, no matter how complicated the constrained space is, to implement the Gibbs sampler after specifying the full conditional posterior distributions of the parameters [15]. Another implementation of sampling from a truncated distribution is to ignore the constraints until the end and then use only the values that satisfy the constraints [16]. However, this scheme becomes very inefficient when the dimensionality of the parameter space is large.

The criteria that we proposed for constraining the HRF are by no means complete. But we opted not to commit ourselves fully until the hemodynamic response mechanisms are fully understood. We try to keep the constrained space as flexible as possible but also respect the main findings of the related theoretical and experimental studies. In summary, we present a general method to use the domain knowledge in the form of parameter constraints and incorporate them into the GLM analysis. These criteria

can obviously be adjusted as our knowledge on HRF dynamics improves.

The whiteness assumption about the noise vector is certainly a simplification. In a recent study [23], the severity of the effects of non-white noise on the inference from fMRI signals was reiterated. The characteristics of the noise in fMRI signals is well-studied and a number of models have been proposed, the most widely used being the autoregressive one [20, 28]. However, the noise in fNIRS signals has not been investigated in detail, yet. Although it may be conjectured that the models proposed for fMRI may also be valid for fNIRS, to be able to keep our expositions simple and to put the emphasis on the comparison between OLS and constrained solutions we assumed the noise vector is white.

5 Conclusions

We have shown that constraining GLM analysis by delimiting ranges of parameters can be beneficial in attaining more realistic HRF waveform estimates. A 3-dimensional volume of permissible parameter values of the canonical basis set acts as prior distribution in the Bayesian analysis, and Gibbs sampling in this volume is used to infer upon the parameters of interest. This procedure, on one hand, eliminates unrealistic HRF waveforms, and on the other hand, it is found to be more effective in identifying activations from noisy signals. One way to improve the proposed scheme is to mitigate the computational complexity arising from the Monte Carlo sampling search. In this respect, we plan to investigate more effective methods to generate samples from truncated distributions. Furthermore we intend to find analytical probability distributions for the constrained space of parameters. This may substantially reduce the computational needs. Finally the search for new basis sets, which cover the space of feasible HRF waveforms more effectively, remains to be explored.

References

1. Akin A, Bilensoy D, Emir UEE, Gülsoy M, Candansayar S, Bolay H (2006) Cerebrovascular dynamics in patients with migraine: near-infrared spectroscopy study. Neurosci Lett 400:86–91
2. Akgül CB, Akin A, Sankur B (2006) Extraction of cognitive activity-related waveforms from functional near-infrared spectroscopy signals. Med Biol Eng Comput 44:945–958
3. Buxton R, Wong E, Frank L (1998) Dynamics of blood flow and oxygenation changes during brain activation: the balloon model. Magn Reson Med 39:855–864
4. Buxton RB, Uludağ K, Dubowitz DJ, Lin TT (2004) Modeling the hemodynamic response to brain activation. Neuroimage 23:S220–S233
5. Cope M, Delpy DT (1998) A system for the long-term measurement of cerebral blood and tissue oxygenation in newborn infants by near infra-red transillumination. Med Biol Eng Comput 26:289–294
6. Devroye L (1986) Non-uniform random variate generation. Springer, New York
7. De Zwart JA, Silva AC, Van Gelterenn P, Kellman P, Fukunaga M, Chu R, Koretsky AP, Frank JA, Duyn JH (2005) Temporal dynamics of the BOLD fMRI impulse response. Neuroimage 24:667–677
8. Dunson DB, Neelon B (2003) Bayesian inference on order-constrained parameters in generalized linear models. Biometrics 59:286–295
9. Ehlis AC, Herrmann MJ, Wagener A, Fallgatter AJ (2005) Multi-channel near-infrared spectroscopy detects specific inferior-frontal activation during incongruent Stroop trials. Biol Psychol 69:315–332
10. Fabbri F, Sassaroli A, Henry ME, Fantini S (2004) Optical measurements of absorption changes in two-layered diffusive media. Phys Med Biol 49:1183–1201
11. Firbank M, Okada E, Delpy DT (1998) A theoretical study of the signal contribution of regions of the adult head to near-infrared spectroscopy studies of visual evoked responses. Neuroimage 8:69–78
12. Friman O, Borga M, Lundberg P, Knutsson H (2003) Adaptive analysis of fMRI data. Neuroimage 19:837–845
13. Friston KJ, Fletcher P, Josephs O, Holmes A, Rugg MD, Turner R (1998) Event-related fMRI:Characterizing differential responses. Neuroimage 7:30–40
14. Friston KJ, Josephs O, Zarahn E, Holmes AP, Rouquette S, Poline JB (2000) To smooth or not to smooth? Bias and efficiency in fMRI time-series analysis. NeuroImage 12:196–208
15. Gelfand AE, Smith AFM, Lee TM (1992) Analysis of constrained parameter and truncated data problems using sampling. J Am Stat Assoc 87:523–532
16. Gelman AB, Carlin JS, Stern HS, Rubin DB (1995) Bayesian data analysis. Chapman & Hall/CRC, Boca Raton
17. Handwerker DA, Ollringer JM, D'Esposito M (2004) Variation of BOLD hemodynamic responses across subjects and brain regions and their effect on statistical analyses. Neuroimage 21:1639–1651
18. Huppert TJ, Hoge RD, Diamond SG, Franceschinini MA, Boas DA (2006) A temporal comparison of BOLD, ASL, and NIRS hemodynamic responses to motor stimuli in adult humans. Neuroimage 29:368–382
19. MacLeod C (1991) Half a century of research on the stroop effect: an integrative review. Psychol Bull 109:163–203
20. Purdon PL, Weisskoff RM (1998) Effect of temporal autocorrelation due to physiological noise and stimulus paradigm on voxel-level false-positive rates in fMRI. Human Brain Mapp 6:239–249
21. Schroeter ML, Zysset S, Wahl M, von Cramon DY (2004) Prefrontal activation due to Stroop interference increases during development –an event-related fNIRS study. Neuroimage 23:1317–1325
22. Smith AFM, Roberts GO (1993) Bayesian computation via the Gibbs sampler and related Markov Chain Monte Carlo methods. J R Stat Soc Ser B (Methodological) 55:3–23
23. Smith AT, Singh KD, Balsters JH (2007) A comment on the severity of the effect of non-white noise in fMRI time-series. Neuroimage 36:282–288
24. Steinbrink J, Villringer A, Kempf F, Haux D, Boden S, Obrig H (2006) Illuminating the BOLD signal: combined fMRI-fNIRS studies. Magn Reson Imaging 24:495–505
25. Suzuki M, Miyai I, Ono T, Kubota K (2008) Activities in the frontal cortex and gait performance are modulated by preparation. An fNIRS study. Neuroimage 39:600–607

26. Villringer A, Chance B (1997) Non-invasive optical spectroscopy and imaging of human brain function. Trends Neurosci 20:4435–4442
27. Woolrich MW, Behrens TEJ, Smith SM (2004) Constrained linear basis sets for HRF modeling using Variational Bayes. Neuroimage 21:1748–1761
28. Woolrich MW, Ripley BD, Brady M, Smith SM (2001) Temporal autocorrelation in univariate linear modeling of fMRI data. Neuroimage 14:1370–1386
29. Worsley KJ, Taylor JE (2006) Detecting fMRI activation allowing for unknown latency of the hemodynamic response. Neuroimage 29:649–654
30. Zysset S, Muller K, Lohmann G, von Cramon DY (2001) Color–word matching Stroop task: separating interference and response conflict. Neuroimage 13:29–36